



## **Structural design of the cable-net and fabric formed, ferrocement sandwich shell roof of NEST HiLo**

Diederik VEENENDAAL<sup>\*</sup>, Jack BAKKER<sup>a</sup>, Philippe BLOCK<sup>b</sup>

<sup>\*</sup>ETH Zurich, Institute of Technology in Architecture, Block Research Group  
Stefano-Franscini-Platz 5, HIL H 46.2, 8093 Zurich, Switzerland  
veenendaal@arch.ethz.ch

<sup>a</sup>ZJA Zwarts & Jansma Architects, Amsterdam, Netherlands

<sup>b</sup>ETH Zurich, Institute of Technology in Architecture, Block Research Group

### **Abstract**

This paper describes the geometry and structural design of a cable-net and fabric formed, ferrocement sandwich shell roof, as part of the NEST HiLo project, to be built in Dübendorf, Switzerland, in 2016. The computational design process consists of an integrated parametric model used for multi-objective evolutionary shape optimisation of the shell, and subsequent analysis of its nonlinear behaviour.

**Keywords:** form finding, optimisation, shell, flexible formwork, sandwich structure, ferrocement

### **1. Introduction**

Thin-shell concrete structures are structurally efficient systems for covering large areas. However, their construction has seen a sharp decline since their golden era, between the 1920s and early 1960s, with the possible exception of air-inflated domes. Commonly cited reasons for their disappearance are the cost of formwork, and the rising cost of associated labour, and the declining interest from architects, possibly related to the limitations of geometries suitable to shell structures (Meyer and Sheer [5]). This paper details the structural design and optimisation for a new concrete shell roof that addresses these issues. The project aims to reduce construction cost and increase attractiveness of shell design and is designed such that it can be constructed with a reusable and lightweight cable-net and fabric formwork system (Veenendaal and Block [12]).

### **2. Context**

This paper describes the geometry and structural design of the HiLo roof at the final design stage prior to detailed engineering and tendering i.e. the 'Bauprojekt' stage in Swiss code SIA 102. HiLo is a research & innovation unit for NEST [7] demonstrating ultra-lightweight construction and active



Figure 1: Visualisations from final design stage of HiLo (renders by Doug&Wolf).

building systems (Figure 1). It is planned as a 16m×9m duplex penthouse apartment for visiting faculty of Empa and Eawag to be completed in 2016 in Dübendorf, Switzerland. HiLo is a collaborative effort of the Block Research Group (BRG) and the Architecture and Building Systems Group (A/S), both at the Institute of Technology in Architecture, ETH Zurich, joined by architectural offices Supermanoeuvre and ZJA Zwarts & Jansma Architects. Structural engineers for the project are Bollinger + Grohmann Ingenieure. HiLo introduces several innovations, and this paper focuses on the development of the roof.

### 3. Description

The roof of HiLo is an anticlastic, thin shell structure to be constructed using a prestressed cable-net and fabric formwork. The shell features spans in the range of 6-9m and is supported on five 'touch-down' points with free edges along its entire perimeter. The shell is built up as a sandwich composite consisting of ferrocement or textile-reinforced concrete faces, and a polyurethane (PU) core.

#### 3.1. Anticlastic shell structure

Typical anticlastic shells are hyperbolic paraboloids, or hypars, which include some of the thinnest known shell structures, particularly those of Félix Candela. These shapes are ruled surfaces, exploiting the use of straight timber in their formworks. Slight improvements to their geometry can drastically improve their structural behaviour (Tomás and Martí [10]). Such deviations can be achieved by using a cable-net and fabric formwork system (Veenendaal and Block [12]) allowing the roof of HiLo to depart from the traditional hypar. Unlike historical hypars, HiLo's roof shell does not have edge beams, but features thin edges, thickening towards the five supports. The shell is not supported by the façade mullions, which only transmit horizontal wind loads to the shell.

#### 3.2. Roof section

The shell is subject to strict requirements for energy performance. The required U-value is 0.17 W/mK and the overall apartment is supposed to generate a 50% annual exergy surplus. The roof is used as a solar collector for electrical and thermal energy on the outside, and as a low energy radiant heating and cooling system on the inside, requiring the inside concrete surface to remain exposed. To minimise thermal bridging, the connection between the glass façade and shell led to the present

sandwich design (Figure 2). Although intuitively the sandwich would seem to present only structural benefits by increasing structural depth and reducing sensitivity to external loads and imperfections, the differences in temperature and humidity on either side of the PU core lead to higher thermal loads and differential strains due to creep and shrinkage.

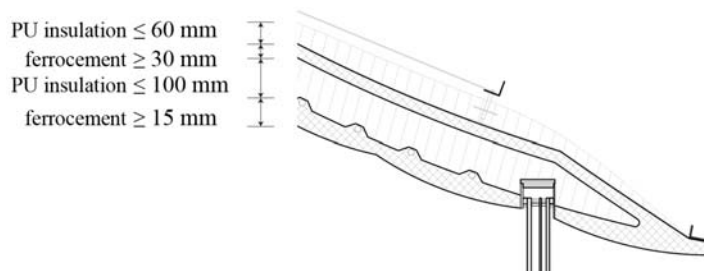


Figure 2: Schematic roof section of HiLo (adapted from drawing by Supermanoeuvre).

### 3.3. Reinforcement

Due to the thinness of the shell and various unfavourable load cases and combinations, the shell will locally act in bending and thus needs to be reinforced accordingly. Ferrocement will allow us to maintain thinness, by following curvatures more easily than traditional rebar, and requiring only minimal cover of 2mm (American code ACI 549R-97). Compared to conventional reinforced concrete, ferrocement has a fine mortar matrix with distributed reinforcement leading to high ductility with homogenous, isotropic properties (including high tensile strength), as well as high durability due to very small crack widths and spacing (Naaman [6]). Textile-reinforced concrete (TRC) with glass or carbon fibre offer similar benefits, but due to its high in-plane thermal conductivity, ferrocement is currently favoured as reinforcement for the thermally active roof.

### 3.4. Cable-net and fabric formwork

The shell is anticlastic everywhere, as it will be constructed on a prestressed cable-net formwork with fabric shuttering, which is lightweight and easily transported. Without the need for scaffolding directly underneath, there is no need for temporary foundations and unobstructed access is made possible. Three historical examples of cable-net formed roofs have been found, dating from the early 1960s (Flint and Low [1], Waling *et al.* [14]). In these cases, substantial deviations from the design shape due to deflections are reported. Van Mele and Block [11] presented a method for finding the distribution of forces to obtain a particular shape, after it has been loaded with fresh concrete. This control allows a range of pre-defined, non-analytical, anticlastic shapes to be designed and constructed, with much greater accuracy (Veenendaal *et al.* [13]).

## 4. Form finding and optimisation process

The design process for the roof consists of an integrated parametric model used for multi-objective evolutionary optimisation of the shell, and subsequent analysis of its nonlinear behaviour as well as the flexible formwork used for its construction. Figure 3 explains the computational design process of HiLo, consisting of form generation, structural analysis, and multi-criteria shape optimisation.

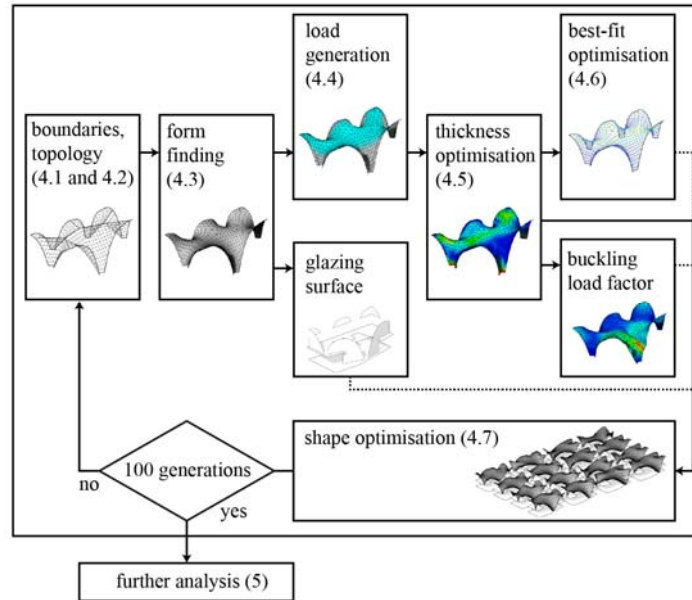


Figure 3: Workflow of optimisation and analysis (sections in parentheses), additional criteria in dotted lines.

#### 4.1. Boundary generation

The shape of the roof is largely determined by the geometry of its boundary edges, and the topology of the generating cable net. The edge consists of five undulations, one for each support, curving between each support position to the given height  $h$  of the roof. Each half undulation is characterised by an amplitude  $a = h$ , period  $p$ , and sharpness  $s$  (Figure 4):

$$z(t) = a \cos^2\left(t(x) \frac{\pi}{2p}\right), \text{ where } t(x) = \frac{s \cdot x + x}{s \cdot x + 1}. \quad (11)$$

In a first optimisation, the five support positions, determining  $p$ , and the sharpnesses  $s$ , were parameters for the optimisation, i.e. ten variables for optimisation.

The boundary curves can extend below the foundation and can optionally be cut off. By doing this, the roof touches down on the floor with a planar, curved footprint. These are defined as parabolas with a certain width  $w$  and depth  $d$ ; two additional parameters for the edge shape (Figure 4). The resulting space is required for the exterior insulation, drainage, connections to the thin-film photovoltaics and hydronic system, providing effective area for the supports, and ensuring that the glass façade connects to the shell at angles of  $\pm 45^\circ$  to allow for proper detailing.

In this case, the sharpness  $s$  can be determined from a height  $h$ , period  $p$ , width  $w$  and amplitude  $a$ :

$$s = -\frac{c + \pi n}{n(c + 2\pi n - \pi)} \text{ where } c = \arccos(2h/a - 1) \text{ and } n = \frac{1}{2} \frac{w}{p} \quad (2)$$

In the final optimisation, the five support positions were fixed, leaving three parameters for optimisation: width  $w$ , amplitude  $a$ , depth  $d$ , i.e. fifteen variables for optimisation.

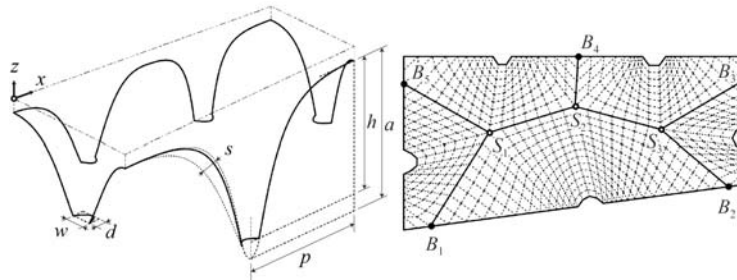


Figure 4: Boundary (left) and topology (right) generation.

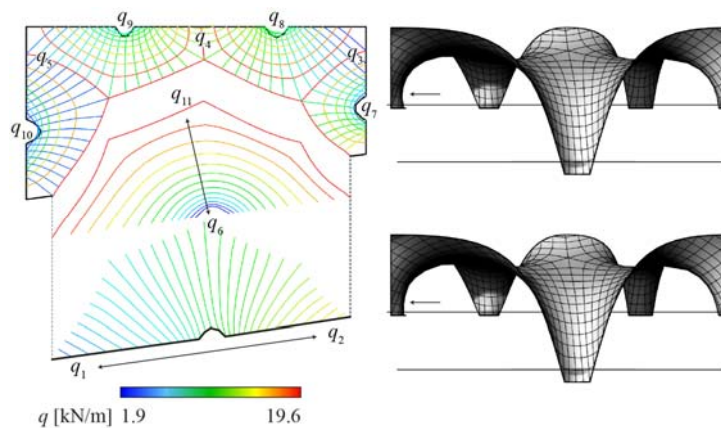


Figure 5: Force densities interpolated from eleven values (left), and constrained mesh (bottom right) to avoid inward curving (top right).

#### 4.2. Topology generation

The roof is then divided into five convex patches, determined by five points  $B_i$  on the shell's boundary and three interior points  $S_i$  (Figure 4). Each patch is then subdivided further along approximately radial and concentric directions with respect to the support positions.

The interior edges of the patch are divided into an equal number of segments that are as close as possible to some desired, global edge length. This same number then subdivides the exterior edges of the patch. The resulting vertices are connected to the corresponding vertices along the interior edges.

Starting at the outermost exterior vertices, concentric edges are created that follow the interior boundary of the patch, crossing all radial edges in between. For undulations that are cut off, the

exterior vertices are divided evenly over the three exterior curve segments, based on their relative lengths. The parabolic segments get at least three vertices, to avoid degrading them into straight lines.

#### 4.3. Form generation

From these boundary conditions, a suitable, anticlastic shape is generated using the linear force density method (Schek [9]). To minimise the number of additional variables for optimisation, the force densities throughout the cable net are determined by interpolating eleven values (Figure 5). The ratio of allowable force densities is limited to 1:20, to create reasonable shapes without too abrupt changes in curvature and resulting forces. In the case of cut off supports, the cable net potentially curves in on itself (Figure 5). This is remedied by calculating force densities of the cable net's triangulated projection using the linear natural force density method (Paulette and Pimenta [8]). This tends towards a minimal surface of our projection, avoiding overlaps, and thus any inward curving. These force densities are then used in a second form-finding procedure, which is also partially constrained to the original form-found mesh.

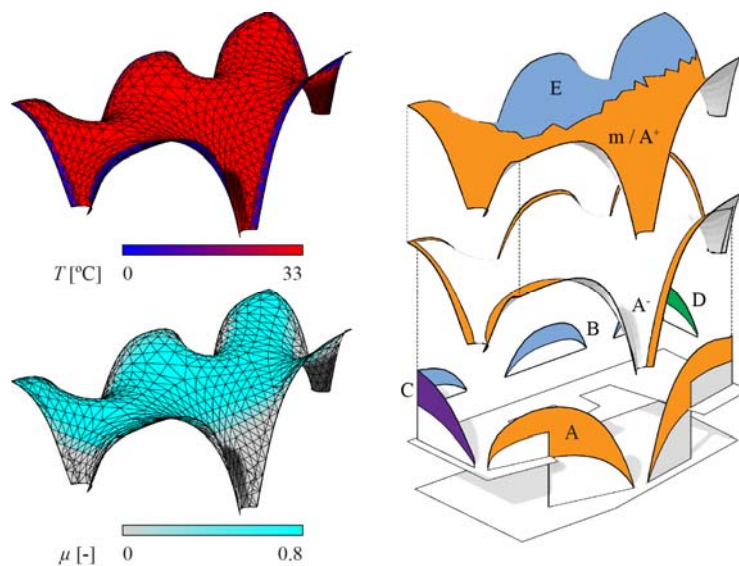


Figure 6: Load generation for thermal loads, snows loads and wind zones for main wind direction (SW) both for pressure (+) and suction (-)

#### 4.4. Load generation

For each shape, loads are automatically generated from SIA 261 to be applied to the structure. These loads include: the self-weight of the concrete (24 kN/m<sup>3</sup>); dead loads from the integrated shell (0.5 kN or 0.3 kN/m<sup>2</sup>); live loads for maintenance on the roof (1 kN or 0.4 kN/m<sup>2</sup>); thermal loads due to the embedded hydronic system for a minimum temperature of 0 °C for optimisation (Figure 6) and -20 °C for final analysis; snow loads ( $\mu \times 0.9$  kN/m<sup>2</sup>, Figure 6), and; wind loads ( $C_p \times 1.07$  kN/m<sup>2</sup>). For the wind loads, half of the wind load on the glass facade is also taken into account. The snow shape factor  $\mu$  varies between 0 and 0.8 depending on the roof angle and the wind shape factor varies between -0.3

and +0.75 depending on the wind direction and roof angle (we interpolate between façade and angled roof, i.e. zone A+ and m, in Figure 6).

Load combinations were defined using reduction factors  $\psi$  and load factors  $\gamma$  in Figure 7. The quasi-permanent load combination is used for the determination of creep and shrinkage, with dead loads and thermal loads altered (0.7 and 0.2) to reflect the actual long-term load on the shell. The occasional load combinations are used for checks in the serviceability limit state (SLS) against allowable deflections and crack width. They are also the starting point for limit load calculations. The ultimate limit state (ULS) load combinations are used to check against allowable stresses. Limit load calculations were carried out to establish whether the load factor  $\lambda$ , or safety factor, according to IASS 1979 was met. This limit load state is here referred to as the critical limit state (CLS).

Load	Self-weight	Dead	Thermal	Live	Wind	Snow
SLS occasional $1.0 / \psi_0$	1.0	1.0 / 0.0	1.0 / 0.6	1.0 / 0.0	1.0 / 0.6	1.0 / 0.86
SLS frequent $\psi_1$ and $\psi_2$	1.0	1.0 / 0.0	0.5 / 0.0	0	0.5 / 0	0.43 / 0
SLS quasi-permanent $\psi_2$	1.0	0.7 (1.0)	0.2 (0.0)	0	0	0
ULS load factor $\gamma$	1.35 / 0.8	1.35 / 0.8	1.50 / 0	1.50 / 0	1.50 / 0	1.50 / 0
CLS load factor $\lambda$	1.75					

Figure 7: Reduction factors  $\psi$ , unfavourable/ favourable load factors  $\gamma$  (SIA 260) and critical buckling load factor  $\lambda$  (IASS 1979).

	Load	Self-weight	Dead	Thermal	Snow	Wind suction	Wind pressure	Live
SLS qp.	LC 0	1.0	0.7	0.2 / 0				
SLS occ.	LC 1	1.0	1.0	1.0 / 0	1.0			
	LC 2	1.0		1.0 / 0		1.0		
	LC 3	1.0		1.0 / 0			1.0	
	LC 4	1.0	1.0	1.0 / 0	0.86			1.0
ULS	LC 5	1.35	1.35	0.6 / 0	1.5			
	LC 6	0.80		0.6 / 0		1.5		
	LC 7	0.80		0.6 / 0			1.5	
	LC 8	1.35	1.35	0.6 / 0	0.86			1.5

Figure 8: Load combinations with and without thermal loads (LC) used.

#### 4.5. Thickness optimisation

By redistributing the material in the shell, it is possible to reduce the total volume of required concrete, even though the maximum stresses stay within the same limits. The program Karamba tries to approach a given maximum deflection of  $L/500 = 18$  mm, while reducing thicknesses throughout the structure and keeping within a 20 MPa stress limit. The linear elastic stiffness was reduced to only  $E = 5000$  MPa to approximately account for cracking and creep in the design. The optimisation is done for all SLS load combinations, as those in the ULS were found to not govern the results. The

presented result has an minimum and average thickness of 3.0 and 7.7 cm, and a total weight of 29 metric tons.

#### 4.6. Best-fit optimisation

The goal is to find the forces such that, under given loads of the wet concrete, the resulting concrete shell takes the form of the target shape (Van Mele and Block [11]). To enforce reasonable bounds on these forces under load (4-50 kN along the perimeter), the resulting constrained linear least squares problem can be written as a quadratic program. Assuming the bounds have not allowed us to find an exact match with the target shape, we compute the sum of squared deviations, which are used as target for optimisation.

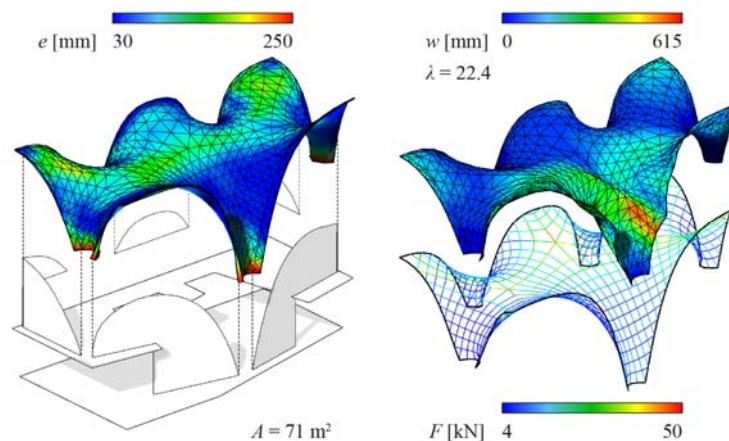


Figure 9: Four criteria: elastic energy (proportional to mass, shown as thickness  $e$ ), buckling load factor  $\lambda$  for LC 0 (showing first positive buckling mode with deflection  $w$ ), cable-net deviations (showing constrained forces  $F$  under load), and surface area  $A$  of clear glazing.

#### 4.7. Shape optimisation

The roof was optimised in two rounds: initially, a single-criterion optimisation (minimising mass subject to stress and deflection constraints), with 21 variables, to study different boundary conditions (positions and number of supports); and, then a final multi-criteria optimisation with 26 variables, to determine the final design. The four criteria were internal elastic energy (proportional to mass), buckling load factor (lowest, positive value), deviation of cable net to target shape, and surface area of glazing. A fifth measure of the amount of head clearance below the roof was also calculated to compare results. The optimisation was carried out for a monolithic concrete shell, and the sandwich section was taken into account in the subsequent structural analysis.

### 5. Structural analysis

The subsequent structural calculations, carried out in Sofistik, follow Swiss code SIA 262 - intended for conventional reinforced concrete - where possible, but applies ACI 549R-97 and ACI 549.1R-93 for aspects related to ferrocement and Medwadowski *et al.* [4], here referred to as 'IASS 1979', for

aspects related to thin-shell structural design. Creep and shrinkage formulas from SIA 262 are based on those in EN 1992-1-1:2004. Adopting IASS 1979 means that we are required to perform a stability analysis, by calculating the initial buckling load, or critical load, then modifying this load - or recalculating using a sufficiently refined model - by taking into account: large displacements (geometric nonlinearity), material properties of concrete and reinforcement (material nonlinearity including creep and shrinkage) and deviations from the idealised shape (imperfections). Because the research unit will be replaced after 5-10 years, the reference period for design is 20 years. Load combinations are according to Section 4.4.

### **5.1. Boundary conditions**

As mentioned, the shell is supported on five locations. Those at the rear are close to the backbone, and assumed fixed. Those in front are supported on a cantilevering, prestressed concrete floor slab, which are modelled as springs (stiffnesses provided by structural engineers of the NEST building, Dr. Schwartz Consulting). One support is modelled as a horizontal spring as well to account for the local flexibility of the supporting steel frame.

### **5.2. Material properties**

The concrete is modelled as a C90/105 with B500A according to SIA 262. The concrete strength is mainly chosen based on the resulting creep and shrinkage behaviour according to code, and given previous experience with viscous and fine concrete mixes, which exhibit high strength (Veenendaal and Block [12]). The steel type is chosen based on its similarity to that mentioned in ACI 549.1R-93. The PU is modelled based on linear elastic properties from suppliers:  $E = 300 \text{ MPa}$ ,  $f_y = 20 \text{ MPa}$ ,  $\gamma = 600 \text{ kg/m}^3$ .

The creep coefficients are  $\phi = 0.91$  (inner face), 2.25 (PU foam insulation) and 0.71 (outer face). The shrinkage strains are  $\varepsilon = -0.38\text{‰}$  (inner face),  $-0.39\text{‰}$  (outer face). This assumes that the shell remains in the formwork while curing for 56 days, that the average layer thickness is 50mm. The inner face is exposed on one side and has a relative humidity of 40%, while the outer face is completely enclosed and has a relative humidity of 60%. For the creep of the PU very little is known, and for now is taken from Garrido *et al.* [2], who investigated rigid PU foam for sandwich panels, though of much lower density.

### **5.3. Limit states**

In SLS, allowable deflections for occasional live loads are  $1/500^{\text{th}}$  of the span  $L$ , i.e. 18mm for the shell, and  $1/300^{\text{th}}$  of twice a cantilever, i.e. 60mm for the cantilevering slab supporting the shell at the front (SIA 260). Deflections along the glass façade are chosen to be less than 10mm. Crack width may not exceed 0.1mm according to ACI 549R-97. In ULS, stresses should not exceed the material strengths (Section 5.1) and buckling may not occur. In CLS, a limit load of more than 1.75 the SLS load combinations should be reached.

### **5.4. Imperfections**

It is assumed that the initial imperfection has the same shape as the first positive, globally acting buckling mode, with a magnitude of 39mm. The initial imperfection  $w_0$  is simply the sum of the calculable imperfection  $w_0'$  and the accidental imperfection  $w_0''$  (IASS 1979). The former is the maximum deflection obtained for a service load combination using linear elastic analysis. As an upper

limit we can take the allowable deflection  $w_0' = 18\text{mm}$  (Section 5.3). The latter is the accidental imperfection due to erection inaccuracies, according to Medwadowski [3]:

$$w_0 = w_0' + w_0'' = 39\text{mm}, \quad (33)$$

where  $w_0'' = 0.1e \left( 1 + \frac{5a}{1 + \beta^{-2}} \right) = 21\text{mm}$ , with  $\beta = 0.001 \frac{\sqrt{R_1 R_2}}{e} = 0.13$ ,

in which  $a = 6$  for a shell built using slipform (assumed to be similar to the cable-net formwork, while  $a$  would be 1 for rigid formworks),  $e$  is the shell thickness, and  $R_1$  and  $R_2$  are the principal radii of curvature of the shell. It is assumed that the (area weighted) mean values can be taken, meaning that the thickness of the sandwich  $e = 140\text{mm}$ , and principal radii  $R_1$  and  $R_2$  are 25m and 14m respectively.

## 6 Results

Figure 11 shows the results from the initial broader optimisation varying position, height and number of supports, identifying greatest potential for structural and energy performance. Figure 12 shows the results from the final multi-criteria optimisation, weighing structural and energy performance against constructional considerations. Figure 13 shows the result for LC 4 without thermal loads, demonstrating that the shell is insensitive to imperfections, features no decreasing post-buckling behaviour, and has a reduced capacity after 20 years of creep and shrinkage.

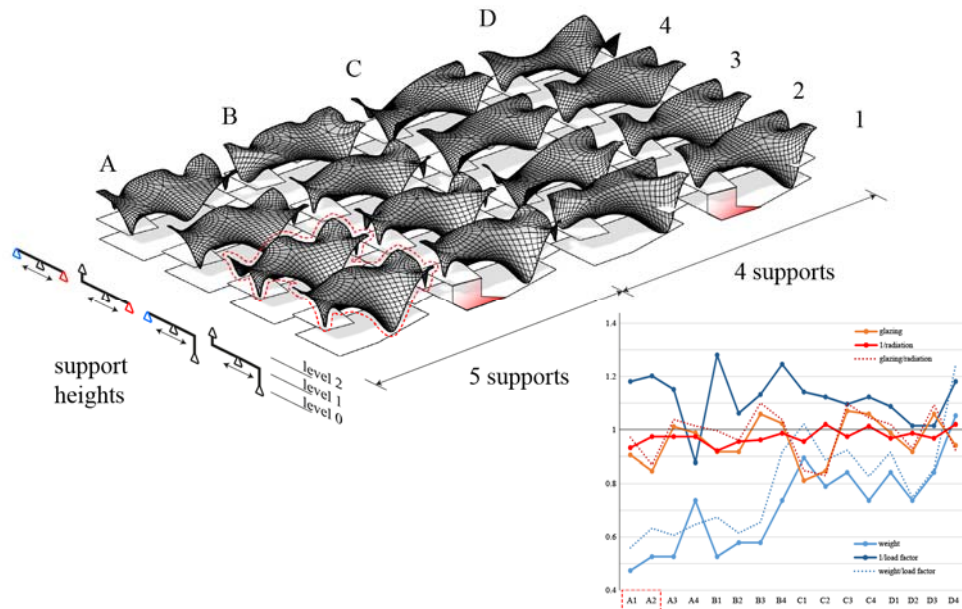


Figure 11: Results from sixteen early optimisations (16x 100 generations, 100 shells each), with A1 and A2 selected for further development based on overall structural and energy performance.

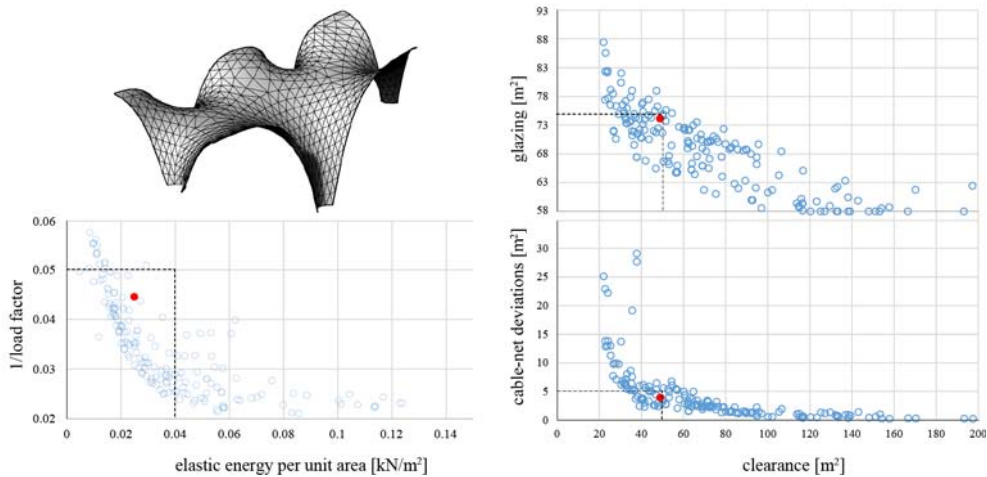


Figure 12: Projections of Pareto front from final multi-criteria optimisation based on buckling load factor, elastic energy (proportional to mass), cable-net deviations, and glazing, showing a measure of head clearance below the roof as well. Limits on variables shown as dotted lines. Final design shown in red.

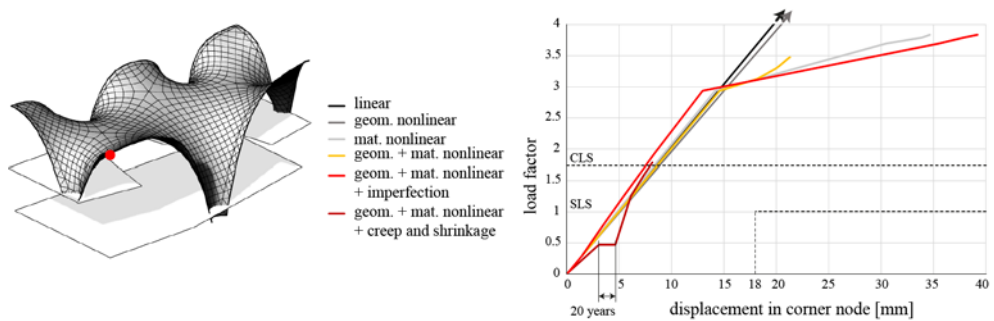


Figure 13: Load-deflection diagram for corner point for LC 4 without thermal loads, showing influence of various nonlinearities.

## 7 Conclusions

The structural design and geometry for the final design of a cable-net and fabric formed, ferrocement sandwich shell roof, as part of the NEST HiLo project, has been presented, and will be handed over to Bollinger + Grohmann Ingenieure for detailed engineering in the next phase. Construction details will be dependent on further development within the design team and outcome of the tendering phase. The final design shown here is the specific result of a sequence of single- and later multi-criteria evolutionary optimisation, evaluating various parameters related to structural and energy performance, as well as architectural, spatial and constructional constraints. Further engineering was carried out to incorporate additional nonlinearities necessary to assess the strength, stiffness and stability of the shell according to Swiss codes, American codes for ferrocement, and IASS recommendations for concrete shells. Meanwhile, the optimisation process and NEST HiLo's unique geometry demonstrate the

potential of greater design freedom for anticlastic shell structures when using a cable-net and fabric formwork. The final construction of NEST HiLo, planned for 2016, will allow the evaluation of other objectives, particularly cost efficiency and energy performance.

## References

- [1] Flint A.R. and Low A.E., The construction of hyperbolic paraboloid type shells without temporary formwork. *Bulletin of the International Association for Shell Structures*, 1960; (4); 5-18.
- [2] Garrido M., Correia J.R., Branco F.A. and Keller T. Creep behaviour of sandwich panels with rigid polyurethane foam core and glass-fibre reinforced polymer faces: Experimental tests and analytical modelling. *Journal of Composite Materials* 2014; **48** (18): 2237-49.
- [3] Medwadowski S.J., Buckling of concrete shells: an overview. *Journal of the International Association for Shell and Spatial Structures*, 2004; **45**(1): 51–63.
- [4] Medwadowski, S.J. et al. *Recommendations for Reinforced Concrete Shells and Folded Plates*. International Association for Shells and Spatial Structures, 1979.
- [5] Meyer C. and Sheer M.H., Do concrete shells deserve another look? Industry professionals give mixed opinions. *Concrete International*, 2005; October; 43-50.
- [6] Naaman, A.E., *Ferrocement and Laminated Cementitious Composites*. Techno Press, 2000.
- [7] *NEST - Exploring the future of buildings*. 2015. [ONLINE] Available at: <http://nest.empa.ch/en/>. [Accessed 26 May 15].
- [8] Pauletti R.M.O. and Pimenta P.M., The natural force density method for the shape finding of taut structures, *Computer Methods in Applied Mechanics and Engineering*, 2008; **197**; 4419-4428
- [9] Schek H.-J., The force density method for form finding and computation of general networks. *Computer Methods in Applied Mechanics and Engineering*, 1974; **3**; 115-134.
- [10] Tomás A, Martí P. Optimality of candela's concrete shells, a study of his posthumous design. *Journal of the International Association of Shells and Spatial Structures* 2010; **51**(1): 67–77
- [11] Van Mele T. and Block P., Novel form finding method for fabric formwork for concrete shells. *Journal of the International Association of Shells and Spatial Structures* 2011; **52**(4):217–24.
- [12] Veenendaal D. and Block P., Design process for prototype concrete shells using a hybrid cable-net and fabric formwork. *Engineering Structures* 2014; **75**:39-50.
- [13] Veenendaal D., Bezbradica M., Novak D. and Block P., Controlling the geometry and forces of hybrid cable-net and fabric formworks. *Proceedings of the IASS-SLTE 2014 Symposium*, Brasilia; 2014.
- [14] Waling J., Ziegler E. and Kemmer H., Hy-par shell construction by offset wire method. *Proceedings, World Conference on Shell Structures*. San Francisco, CA, US; 1962; October 1-4; 453-462.